Dynamics of an assembly of finite-size Lennard-Jones spheres

P. Singh
Mail Stop J576, Engineering Sciences and Applications, Energy and Process Engineering, Los Alamos National Laboratory, Los Alamos, New Mexico 87545

(Received 19 May 1995; revised manuscript received 18 December 1995)

The time-averaged Fourier spectra of the number density, velocity, and force fields are obtained numerically for an assembly of spherical particles interacting via the Lennard-Jones potential. The magnitude spectra determine the dominant wave numbers, and the phase difference between the Lennard-Jones force and number density spectra determines the nature of the particle dynamics. The latter is used to show that for every wave number k there is a critical frequency $\omega_c(k)$, such that when $\omega<\omega_c(k)$ the phase difference is $\pi/2$ and when $\omega>\omega_c(k)$ the phase difference is $-\pi/2$. The ratio of the frequency and the wave number at which the phase difference changes sign is used to define an effective sound speed for the particle system. The effective sound speed is shown to be a function of the dimensionless wave number, and is locally minimum at the same dimensionless wave numbers for which the static structure factor is minimum. It is also shown that the dynamical response of the particle system for waves with speeds greater than the effective sound speed is similar to the response of the hyperbolic systems of equations, and for waves with speeds smaller than the effective sound speed the response is similar to the response of the elliptic systems. The convection effects are shown to be of the same order of magnitude as the Lennard-Jones forces, and the change of type of the equations from hyperbolic to elliptic occurs when the magnitude of the convection term is comparable to the magnitude of the Lennard-Jones force term. It is also shown that the change of type cannot occur in a theory where the convection term is neglected. [S1063-651X(96)02106-X]

PACS number(s): 47.35.+i, 05.60.+w

I. INTRODUCTION

A detailed study of the number density, velocity, and force fields of particle systems, e.g., suspensions, simple liquids, etc., is important for the fundamental understanding of the dynamical behavior of these systems. The nature of the number density and velocity fields has been studied extensively in the past, both experimentally by using diffraction techniques and numerically by simulations of model fluids (Verlet [1], Chandler [2], Hansen and McDonald [3], Boon and Yip [4], Pusey [5], Wai *et al.* [6], and Wignall *et al.* [7], see these papers for additional references). These studies have shed considerable light on the mechanisms that are important in determining the microscopic structure of the particle distribution, and have also related the microscopic structure to the macroscopic properties of these systems. Specifically, at length scales comparable to the particle or atomic diameter D, the spatial distribution of particles is nonuniform. The spatial nonuniformity of the particle distribution is quantified in terms of the radial distribution function, which is an oscillating function of the distance from the reference particle, and its Fourier transform. From these studies we also know that there are many common features between the radial distribution functions of fluidized suspensions ($D\sim10^{-2}$–10^{-7} m) and simple liquids ($D\sim10^{-10}$ m), even though the particle diameters differ by several orders of magnitude (also see Gingrich [8], Kruh [9], Yarnell *et al.* [10], Pusey [5] Wai *et al.* [6], Wignall *et al.* [7], Hansen and McDonald [3], Ottewill [11], Boon and Yip [4], Singh [12], and Singh and Joseph [13–15], for a detailed discussion and additional references). The fact that the radial distribution functions of these mechanically different systems are the same suggests that a comprehensive understanding of any one of these systems can also lead to a better understanding of all particle systems.

In this paper, our main goal is to study the structure contained in the spatial and temporal distributions of the number density, velocity, convection, and force fields for an assembly of particles interacting via the Lennard-Jones potential. For a finite number of particles in a periodic domain these distributions were computed numerically by integrating the equations of motion. The particle trajectories and the distributions, in general, are four dimensional, i.e., depend on space and time, and thus the computational effort required to obtain the correlation functions of these distributions are enormous. For isotropic systems, however, the radial symmetry can be exploited by averaging over the solid angle, and accurate estimates of the correlation functions can be obtained from a relatively small data set.

For a particle system the phase of the number density distribution is related to the actual particle positions. The phase, therefore, changes constantly with time as the particles constantly move around in a fluid. Furthermore, for an isotropic system the phase of a distribution by itself is *not* very important because the macroscopic equilibrium properties of these systems are related only to the correlation functions that are independent of the phase. However, our numerical results show that the phase difference between two independent distributions, such as the number density and Lennard-Jones force fields, contains valuable information about the particle dynamics. In particular, we show that the phase difference between the Lennard-Jones force and the number density fields is a function of the wave number and frequency. When $\omega<\omega_c(k)$ the phase difference is approximately $\pi/2$ and when $\omega>\omega_c(k)$ it is approximately $-\pi/2$, where $\omega_c(k)$ is a critical frequency for the particle system that depends on the wave number and the system parameters.

We will show later in this paper that the phase difference between the number density and the Lennard-Jones force fields changes sign at the dimensionless wave numbers for which the convection term is of the same order of magnitude as the Lennard-Jones force term. The critical frequency $\omega_c(k)$ at which the phase difference changes sign can be used to define a characteristic sound speed for the particle system. Our numerical results also show that the qualitative form of the Lennard-Jones force field for $\omega<\omega_c(k)$ is different from its form for $\omega>\omega_c(k)$ and the mathematical type of the governing equations for the particle system changes at $\omega=\omega_c(k)$. Specifically, it is shown that the area-averaged model equations of the particle system for waves with speeds greater than the effective sound speed are hyperbolic, and for waves with speeds smaller than the effective sound speed are elliptic. This is a fundamental change in the model equations because for the elliptic systems the local solution depends on the overall distribution in the domain, but for the hyperbolic systems the local solution depends only on the distribution along the upstream portion of the local characteristic.

In Sec. IV, we will show that in a theory where the convection term is neglected the change of type predicted from the direct numerical simulations cannot occur because the momentum equation in this case contains only two terms, and the number density, velocity, and force spectrums are linearly related. Therefore, the change of type of the Lennard-Jones particle systems can be predicted only in a mathematical model where the nonlinear convection term is included.

Finally, we note that when the correlation functions are obtained for a distribution the phase of the distribution is lost, and therefore the phase difference between two distributions cannot be studied if we *only* have access to their correlation functions. Also note, in general, both the distributions and the phase differences are three-dimensional. For isotropic systems, however, by definition all properties, including the phase difference distribution, must be the same along all directions. Thus the phase difference for an isotropic system can be studied in terms of one-dimensional distributions. We shall see later that this study of the phase difference can be conducted in terms of the one-dimensional area-averaged distributions used by Singh [12] and Singh and Joseph [13–15] in their study of the spatial distribution of particles in fluidized suspensions.

II. THREE-DIMENSIONAL AND ONE-DIMENSIONAL AREA-AVERAGED DISTRIBUTIONS

We begin with a brief description of the three-dimensional distributions and their correlation functions used for describing the spatial arrangement of particles. The number density function specifies the coordinates of all particles in the system.

$$\rho(\mathbf{r},t)=\sum_{i=1}^{n}\delta(\mathbf{r}-\mathbf{R}_i(t)), \tag{2.1}$$

where $\mathbf{r}=\mathbf{R}_i(t)$ is the position vector of the center of the ith particle at time t, n is the number of particles in the system, and δ is the delta function (see Hansen and McDonald [3]). Alternatively, the correlation functions and their Fourier transform can be used to describe their relative spatial arrangement, and the overall structure of the spatial distribution. For example, given a particle at the origin of the coordinate system, the radial distribution function $g(\mathbf{r},t)$ represents the probability of finding another particle at distance $\mathbf{r}$ from the origin. By definition, $g(\mathbf{r},t)$ is given by

$$g(\mathbf{r},t)=\int \rho(\mathbf{r}+\mathbf{r}',t)\rho(\mathbf{r}',t)d\mathbf{r}'. \tag{2.2}$$

Note in obtaining the correlation function, we have *lost* the phase information contained in the number density distribution which, as we shall see later, can be used to obtain important information about the dynamical behavior of the particle systems.

By taking the Fourier transform of the above equation and using the convolution-multiplication theorem, the above relation reduces to

$$g(\mathbf{k},t)=|\rho(\mathbf{k},t)|^2, \tag{2.3}$$

where the dynamic structure factor $g(\mathbf{k},t)$ is the three-dimensional spatial Fourier transform of $g(\mathbf{r},t)$, $\rho(\mathbf{k},t)$ is the Fourier transform of $\rho(\mathbf{r},t)$, and $\mathbf{k}$ is the wave number. In this article, we will use the same symbol to denote the distribution and its Fourier transform, and distinguish between the two by the arguments.

When the time average of the distribution function is radially symmetric it takes the following simplified form:

$$\langle g(|\mathbf{r}|)\rangle=\langle g(\mathbf{r})\rangle=\lim_{T\to\infty}\frac{1}{T}\int_0^T g(\mathbf{r},t)dt, \tag{2.4}$$

where $\langle\ \rangle$ denotes the time average. Also note when $\langle g(|\mathbf{r}|)\rangle$ is radially symmetric a relation similar to (2.3) hold for the time-averaged quantities because the Fourier transformation is a linear operation, i.e.,

$$\langle g(|\mathbf{k}|)\rangle=\langle|\rho(|\mathbf{k}|)|^2\rangle. \tag{2.5}$$

The time average of $g(\mathbf{k},t)$, i.e., $\langle g(\mathbf{k})\rangle$, is called the static structure factor.

Next we define the area-averaged number density $N(z,t)$ on the plane z to be

$$N(z,t)=\int_{-\infty}^{\infty}\int_{-\infty}^{\infty}\rho(\mathbf{r},t)dx\ dy. \tag{2.6}$$

The above mapping between $N(z,t)$ and $\rho(\mathbf{r},t)$ is, in general, not invertible because the detailed information about the x and y coordinates of the particles is lost during the area averaging. However, when the autocorrelation function of $\rho(\mathbf{r},t)$ is radially symmetric, i.e., $g(\mathbf{r},t)=g(|\mathbf{r}|,t)$, it is easy to show that

$$\mathrm{g}(|\mathbf{k}|,t)|=\frac{1}{4\pi^2}|N(k,t)|^2, \tag{2.7}$$

where $N(k,t)$ is the one-dimensional spatial Fourier transform of $N(z,t)$ (see Singh and Joseph [15] for details). Therefore, in this special case the autocorrelation of $N(z,t)$ is equivalent to $g(|\mathbf{r}|,t)$. Also note that when $\rho(\mathbf{r},t)$ is not

radially symmetric, but its time-average $\langle \rho(\mathbf{r},t)\rangle$ is radially symmetric, then a relation similar to (2.7) holds for the time-averaged quantities

$$\begin{aligned}\langle N(k)\rangle &= \lim_{T\to\infty}\frac{1}{T}\int_0^T N(k,t)dt \\ &= \lim_{T\to\infty}\frac{1}{T}\int_0^T\int_z N(z,t)\exp(ikz)dz\ dt \\ &= \lim_{T\to\infty}\frac{1}{T}\int_0^T\int_z\left[\int_x\int_y \rho(\mathbf{r},t)dx\ dy\right]\exp(ikz)dz\,dt \\ &= \int_{\mathbf{r}}\left[\lim_{T\to\infty}\frac{1}{T}\int_0^T \rho(\mathbf{r},t)dt\right]\exp(ikz)dx\,dy\,dz \\ &= \int_{\mathbf{r}}\langle\rho(\mathbf{r})\rangle\exp(ikz)d\mathbf{r} = \int_{\mathbf{r}}\langle\rho(|\mathbf{r}|)\rangle\exp(ikz)d\mathbf{r} \\ &= 2\pi\langle\rho(|\mathbf{k}|)\rangle, \end{aligned} \tag{2.8}$$

where $i=\sqrt{-1}$. Later in this paper, we will use (2.8) for the interpretation of data obtained for our numerical simulations, and also to understand the results of diffraction studies (see the Appendix). A detailed study of the area-averaged distributions is also important because *only* the Fourier transforms of the area-averaged distributions are measured in diffraction studies. Another advantage of working with the area-averaged distribution is that the average momentum balance perpendicular to the averaging plane can be studied in terms of the area-averaged acceleration and forces acting on the particles in that plane.

In order to study the time evolution of the phase difference between two distributions we must work with the distributions, and not their correlations, because when the correlation functions are calculated the phase information is lost. Furthermore, the distributions such as $\rho(\mathbf{r},t)$ and $u(\mathbf{r},t)$ and their phase difference distributions are three dimensional. Therefore for anisotropic systems the phase difference must be studied along three mutually perpendicular directions. For isotropic systems, however, the time average of the phase distribution along the three perpendicular directions must be the same; therefore it is sufficient to study the phase distribution along one fixed direction. The phase distribution of a three-dimensional distribution perpendicular to the averaging plane is preserved in the area-averaged distribution, e.g., the phase of $\rho(\mathbf{r},t)$ along the z direction is preserved in $N(z,t)$, and therefore the phase difference distributions can be studied in terms of the area-averaged distributions, as we do in this paper.

III. EQUATIONS OF MOTION

We begin this section by presenting the governing equations for the particles, and the numerical discretization scheme used to integrate these equations. The momentum conservation equations for the n particles inside the computational domain can be written as

$$m\frac{d\mathbf{u}_i}{dt}=\mathbf{f}_i(t), \quad i=1,\ldots,n, \tag{3.1}$$

when m is the mass of one particle, $\mathbf{u}_i$ is the velocity of the ith particle, and $\mathbf{f}_i(t)$ is the force acting on the ith particle at time t. In a numerical solution, since the locations of all particles in the domain are known, $\mathbf{f}_i(t)$ for a system of Lennard-Jones particles can be computed by evaluating the following expression:

$$\mathbf{f}_i=-\frac{48\epsilon}{D^2}\sum_{j=1}^{n}{}'\ (r_{ij}^{-13}-0.5r_{ij}^{-7})\ \frac{\mathbf{r}_{ij}}{r_{ij}}, \tag{3.2}$$

where ϵ is the depth of the potential well at its minimum, D is the effective Lennard-Jones particle diameter, $\mathbf{r}_{ij}$ is the vector from the particle i to the particle j, and r_{ij} is the magnitude of the vector $\mathbf{r}_{ij}$. Also note that the term $i=j$ is not included in the above summation. We will assume that there are 864 particles inside a cubic computational domain with sides $L=10.229\ D$. This corresponds to a reduced density $\rho^*=(nD^3/L^3)=0.807\,26$. We will also assume $\varepsilon=119.8k_B$, where k_B is the Boltzmann constant, $m=6.63\times10^{-26}$ kg and $D=3.405\times10^{-10}$ m; these values correspond to real Argon.

A fourth order scheme is used to discretize the momentum equations for the particles (see Hansen and McDonald [3] for details). The force acting on the particle i is computed based on all other particles in the computational domain and their periodic images. At each of the six walls of the computational domain, appropriate periodic boundary conditions are imposed. The discretized equations are integrated numerically in time until a steady state is reached. The steady state kinetic energy of the particle system is controlled by increasing or decreasing the particle velocities by a constant factor. After the steady conditions are reached, at each time step the particles' coordinates and velocities, and the forces acting on the particles are recorded in a data file. From this recorded data the correlations of the number density, velocity, convection, and force fields are obtained during the post processing phase. All correlations reported in this paper remained *unchanged* when the time step used in the numerical integration scheme was reduced by a factor of five. Therefore the correlations reported in this paper are independent of the time step used.

Even though a direct numerical solution of the n particle Eq. (3.1) in a periodic computational domain can be easily obtained, it is advantageous to have a model that captures the essential features of the particle system because the macroscopic properties of the particle system can be obtained more easily from the model equations. To develop a model for the particle system we need two equations: one for the conservation of number density and the other for the conservation of momentum. The conservation of number density is given by

$$\frac{\partial\rho}{\partial t}+\nabla\cdot\mathbf{J}=0, \tag{3.3}$$

where $\mathbf{J}(\mathbf{r},t)=\Sigma_{i=1}^{n}\mathbf{u}(\mathbf{r},t)\delta(\mathbf{r}-\mathbf{R}_i(t))$ is the velocity current and $\mathbf{u}(\mathbf{r},t)$ is the velocity of the particle whose center is at $\mathbf{r}$ at time t. The conservation of momentum is given by

$$m\frac{d\mathbf{J}(\mathbf{r},t)}{dt}\equiv m\frac{\partial\mathbf{J}(\mathbf{r},t)}{\partial t}+m\frac{\partial}{\partial x_q}\left[\sum_{i=1}^{n}u_q u_p\mathbf{e}_p\delta(\mathbf{r}-\mathbf{R}_i(t))\right]$$
$$=m\sum_{i=1}^{n}\frac{d\mathbf{u}}{dt}\delta(\mathbf{r}-\mathbf{R}_i(t))\equiv\mathbf{F}(\mathbf{r},\rho). \tag{3.4}$$

Here $\mathbf{F}(\mathbf{r},\rho)$ is the force at $\mathbf{r}$, and $\mathbf{e}_p$ is the unit vector along the p-coordinate axis. In the above equation we have used the notation that implies summation with respect to the repeated indices. We will again assume that the particles interact with each other via the Lennard-Jones potential, and therefore the exact force acting on the particles can be computed when the particles' coordinates are known. The second term on the left hand side of the above equation is the familiar convection term. Note Eq. (3.4) is mathematically equivalent to Eq. (3.1). In fact, we have simply used a compact notation to rewrite the set of n particle Eq. (3.1).

Equations (3.3) and (3.4) are not very useful unless a model is available to independently estimate the average form of the right hand side of (3.4). Several theoretical models have been proposed to estimate the right hand side of (3.4) which have been partially successful in predicting the essential features of the dynamic structure factor (see Hansen and McDonald [3], and Boon and Yip [4] for a detailed discussion and additional references). In these theories, however, the nonlinear convection term is considered to be small and *not* included. It is clear from (3.4) that when the convection term is dropped the force distribution is linearly related to the time derivative of the velocity current which in turn is linearly related to the number density distribution by Eq. (3.3). That is, the equation system (3.3) and (3.4) is linear, and hence its solution can be described in terms of ρ, J, or F. The usual choice is to describe it in terms of the dynamic structure factor $|\rho(k,\omega)|^2$ which can be measured directly in a diffraction study. Also note that in the linear case no additional information can be obtained from the phase difference distributions. In this paper, we obtain the convection and Lennard-Jones force terms from direct numerical simulations which show that the two terms are of comparable magnitude. The phase difference between the Lennard-Jones force and number density distributions is also obtained from the direct numerical simulations. As we have noted earlier, the area-averaged distributions are used in this paper because the phase difference between the distributions can be studied only in terms of the area-averaged distributions.

The governing equations for the area-averaged number density and velocity fields can be easily obtained by averaging Eq. (3.3) and the z component of (3.4) over the $z=$const planes. The mass conservation equation becomes

$$\frac{\partial N}{\partial t}+\frac{\partial J}{\partial z}=0, \tag{3.5}$$

where $J(z,t)=\int_{-\infty}^{\infty}\int_{-\infty}^{\infty}J(\mathbf{r},t)\,dx\,dy$ is the average velocity current along the z direction. The equation for the momentum conservation becomes

$$\frac{\partial J(z,t)}{\partial t}=\left[\sum_{i=1}^{n}\frac{f_z}{m}\delta(z-Z_i(t))\right]-\frac{\partial}{\partial z}\left[\sum_{i=1}^{n}uu\,\delta(z-Z_i(t))\right]$$
$$=\frac{F(z,t)}{m}-\frac{\partial}{\partial z}\left[\sum_{i=1}^{n}uu\,\delta(z-Z_i(t))\right], \tag{3.6}$$

where $F(z,t)$ is the area average of the z component of the forces acting on the particles with $z=Z_i(t)$. Note for the Lennard-Jones particle system, $F(z,t)$ depends *only* on the instantaneous particles' centers. i.e. $F(z,t)=F(N(z,t))$. The above equations for the area-averaged distributions are exact, and hence suggest the terms we must model to obtain the time evolution of $J(z,t)$.

The convection terms with derivatives along the x and y directions:

$$\frac{\partial}{\partial x}[u_x uN]\quad\text{and}\quad\frac{\partial}{\partial y}[u_y uN],$$

present in the z component of the momentum equation, drop out when averaging is done over the $z=$const planes. Therefore the area-averaged momentum equation along the z direction is decoupled from the area-averaged momentum equations along the x and y directions. On the other hand, the three components of the momentum equation coupled via the nonlinear convection term are decoupled only when the magnitude of the convection term is negligible compared to the other terms in the momentum equation. Hence it is advantageous to work with the area-averaged equations.

In the remainder of this section, we define the Fourier transforms of all relevant distributions, including those present in Eqs. (3.5) and (3.6). The average forms of the spectra presented in this paper were obtained by averaging over 100 000 samples. The area-averaged longitudinal force spectrum is important because it appears in Eq. (3.6):

$$F(k,\omega)=\sum_{j=1}^{n}f_{zj}(t)\exp[i(kz_j(t)-\omega t)]. \tag{3.7}$$

The transverse force spectrum $F_t(k\omega)$:

$$F_t(k,\omega)=\sum_{j=1}^{n}f_{yj}(t)\exp[i(kz_j(t)-\omega t)], \tag{3.8}$$

is not relevant to the area-averaged equations because it acts in the averaging plane. However since the particle dynamics is actually three dimensional, we will also study its form.

The longitudinal convection spectrum:

$$C_z(k,\omega)=-ik\sum_{j=1}^{n}u_j^2(t)\exp[i(kz_j(t)-\omega t)] \tag{3.9}$$

appears in Eq. (3.6), and therefore is relevant to the particle dynamics. As we have noted earlier, our numerical simulations show that for the Lennard-Jones particle systems its magnitude is *comparable* to that of the Lennard-Jones force term.

The longitudinal current spectrum

$$J(k,\omega)=\sum_{j=1}^{n} u_j(t)\exp[i(kz_j(t)-\omega t)],$$

and the number density spectrum are related by Eq. (3.5), i.e., $ikJ(k,\omega)=i\omega N(k,\omega)$, and therefore it is sufficient to study the distribution of $N(k,\omega)$.

By using the above definitions, we can write the Fourier transform of Eq. (3.6) as

$$i\omega J(k,\omega)=\frac{1}{m}F(k,\omega)-C_z(k,\omega). \tag{3.10}$$

In the next section, the area-averaged momentum Eq. (3.10), and thus also 3.6), is verified by *independently* computing the left and right hand sides for our numerical simulations. It is shown that for the numerical solutions, the averaged spectra of the left and right hand sides are approximately equal and the average phase difference between the terms is 0 or π, as required by Eq. (3.10). The area-averaged Eq. (3.6), therefore, correctly models the key features of the exact momentum conservation.

Here it is also important to note that if the convection term in Eq. (3.10) is dropped then the phase relationship between the velocity current and the Lennard-Jones force is *fixed*. In this degenerate case the phase contains no additional information about the particle dynamics, and can be dropped. However, as we will see later, when the convection term is not negligible the phase difference between the number density and Lennard-Jones force fields is important, but is an unknown to be determined by solving the governing equations, as we do in this paper.

The Fourier spectra we have defined above are complex: therefore, in general, we must study both magnitude and phase of these spectra. However, for the system on hand, the phase spectra are related to the particles coordinates, and therefore no additional information about the particle dynamics can be deduced from the phase spectra. The phase difference between two independent spectra, however, can be used to further understand the particle dynamics. In order to understand this idea, we first study the phase difference between the number density and longitudinal velocity current spectra. This can be easily obtained from Eq. (3.5)

$$\arg(J(k,\omega))-\arg(N(k,\omega))=0$$

where arg( ) is the argument of a complex number. To prove that Eq. (3.5) is satisfied by the numerical simulations we must also show that the above relationship between $\arg(N(k,\omega))$ and $\arg(J(k,\omega))$ holds. The phase difference between $N(k,\omega)$ and $J(k,\omega)$ is fixed because there are *only* two terms in Eq. (3.5).

The momentum equation, however, contains three terms, and thus the relative sign of any two terms can change as the magnitude of the third term changes. A simple analysis of Eq. (3.5) and (3.10) shows that the phase difference between $N(k,\omega)$ and $F(k,\omega)$ must be $\pm\pi/2$, and between $F(k,\omega)$ and $C_z(k,\omega)$ must be 0 or π. Clearly, these conditions must be satisfied by the numerical solution, otherwise the particle system cannot be modeled in terms of these equations. Also note, if $C_z(k,\omega)$ is relatively small, as is the case in the long wave or continuum limit, then the phase difference between $N(k,\omega)$ and $F(k,\omega)$ must be $-\pi/2$. However when the convection term is neglected there are only two terms in Eq. (3.10): $F(k,\omega)$ and $J(k,\omega)$. But, as we have noted earlier, this leads to a relatively simple case because we get $F(k,\omega)=i\omega mJ(k,\omega)$, and hence the *same* information is contained in $F(k,\omega)$, $J(k,\omega)$, and $N(k,\omega)$. Therefore in a theoretical model where the convection term is neglected the dynamic structure factor is sufficient to completely describe the model system. However since our direct numerical simulations for the Lennard-Jones particle systems show that the convection term is not negligible, to completely describe the particle dynamics $N(k,\omega)$ and $F(k,\omega)$, and the phase difference between them, must be known. Here it is important to note that in the diffraction studies, and also in the direct molecular dynamic simulations, the dynamic structure can be obtained directly without any knowledge of $F(k,\omega)$, $C_z(k,\omega)$ or the phase difference. But, as we will discuss in the next section, $F(k,\omega)$, $C_z(k,\omega)$ and the phase difference are essential for understanding the detailed dynamics.

In general, the phase difference between the number density and the Lennard-Jones force spectra P_{FN} is a function of k and ω. For our numerical results, the functional form of P_{FN} is obtained as follows:

$$P_{FN}(k,\omega)\equiv\arg\left[\left\langle\frac{F(k,\omega)}{N(k,\omega)}\frac{|N(k,\omega)|}{|F(k,\omega)|}\right\rangle\right].$$

IV. RESULTS

We have already mentioned in the previous section that the numerical results were obtained by integrating the system of Eqs. (3.1) and (3.2) for the particles in time. The particles' coordinates, velocities and force fields were computed at each time step and recorded in a data file. The Fourier spectra were obtained later by processing this data file. The averaged spectra presented this paper were obtained by averaging over 100 000 samples. The spectra are studied by plotting isovalues in the two-dimensional (k,ω) domain, and when necessary by plotting one-dimensional sections for k or ω fixed.

We begin with a brief discussion of the area-averaged number density spectrum which for an isotropic system, as we have noted earlier, is the same as the square root of the dynamic structure factor (see Sec. III). The dynamic structure factors obtained for this study are the same as in the previous studies (see Boon and Yip, and Hansen and McDonald for a detailed discussion and additional references), and so we will only mention its key features. In Fig. 1(a) we have plotted $|N(k,\omega)|$ for $T=104$ K, and the detailed profiles for $\omega=0$ are shown in Fig. 1(b) for $T=104$ K and 77 K. From these figures we note that for both cases the maximum is for $\omega=0$. The maximum value is smaller for the case with higher temperature, and k at the maximum is slightly smaller for the case with higher temperature; for $T=104$ K the maximum value of 1628 is at $kD=6.59$, and for $T=77$ K the maximum value of 1706 is at $kD=6.61$. Furthermore, for $\omega=0$ there are secondary peaks, but they are not integer multiples of the main peak. From Fig. 1(b), where the static structure factors for the two cases are shown, we note that the dimensionless minima are the same as the set of zeros of the blockage function (see the Appendix). From the isovalue

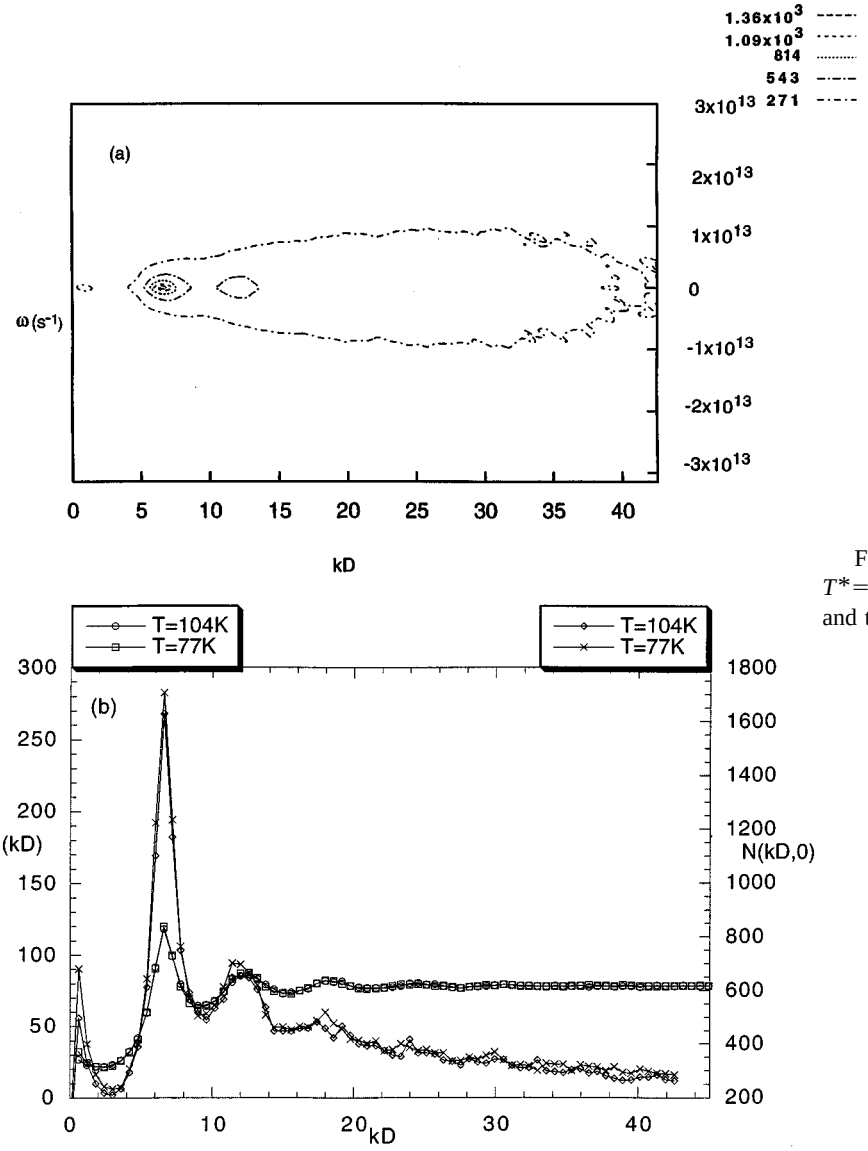

FIG. 1. (a) Isovalues of $|N(k,\omega)|$ for $T^*=0.872$, (b) sections of $|N(k,\omega)|$ for $\omega=0$, and the static structure factors $|N(k)|$ are shown.

plots shown in Fig. 1(a) we also note that the peaks and valleys of $|N(k,\omega)|$ become progressively less pronounced with increasing $|\omega|$. Also note that the numerical results obtained for $kD<(2\pi D/L)$ are sensitive to the size of the computational domain, and hence must be verified by changing the ratio (L/D). In this paper, we will simply ignore the numerical results obtained for $kD<(2\pi D/L)$.

From Eq. (3.6) we know that the time derivative of the local velocity current contains two contributions: one is the Leonard-Jones force field that accounts for the particle-particle interactions, and the other is the convection contribution. The first contribution depends on the positions of the particles, and can be computed *exactly* when the particles' coordinates are known. However, when the particles move the Lennard-Jones forces acting on the particles change, and therefore the spectra of the Leonard-Jones force field depend on the motion of the particles. In the next few paragraphs, we present the spectra of the longitudinal and transverse component of the Lennard-Jones force fields, and then will study the spectra of the convection term.

The averaged Fourier spectrum of $|F(k,\omega)|$ is shown in Fig. 2(a) for $T=104$ K and the static Lennard-Jones force spectra $|F(k)|=|\int F(k,\omega)d\omega|$ are shown in Fig. 2(b) for $T=104$ K and 77 K. From these figures we note that the magnitudes of both $|F(k,\omega)|$ and $|F(k)|\rightarrow 0$ in the limit $kD\rightarrow 0$, which shows that in the long wave limit the Lennard-Jones force acting on the particles approaches zero. We also note that $|F(k,\omega)|$ is a symmetric function of ω, and that there are three maxima of approximately equal magnitudes, two of which are located symmetrically about the k axis and one is on the k axis. The maxima for $T=104$ K are at $\sim(kD=3.30,\ \omega\pm 9.15\times 10^{12}$ s) and $\sim$ $(kD=6.59,\ \omega=0)$. Note that the dominant peaks at $\omega=\pm 9.15\times 10^{12}$ s and $kD=3.3$, correspond to traveling waves with wavelength $\sim 1.90D$. It is interesting to note that the wave number at these dominant peaks is approximately one half of the wave number for the dominant peak of $|N(k,\omega)|$. In addition to these peaks, for $T=104$ K there are secondary peaks at $(kD=12.6,\ \omega=0)$, $(kD=17.40,\ \omega=0)$, and $(kD=9.58,\ \omega=\pm 9.65\times 10^{12}$ s). From these figures we also note that the secondary peaks, for both $\omega=0$ and $\omega\neq 0$, become less pronounced with increasing k. Finally, we note that the positions of the peaks

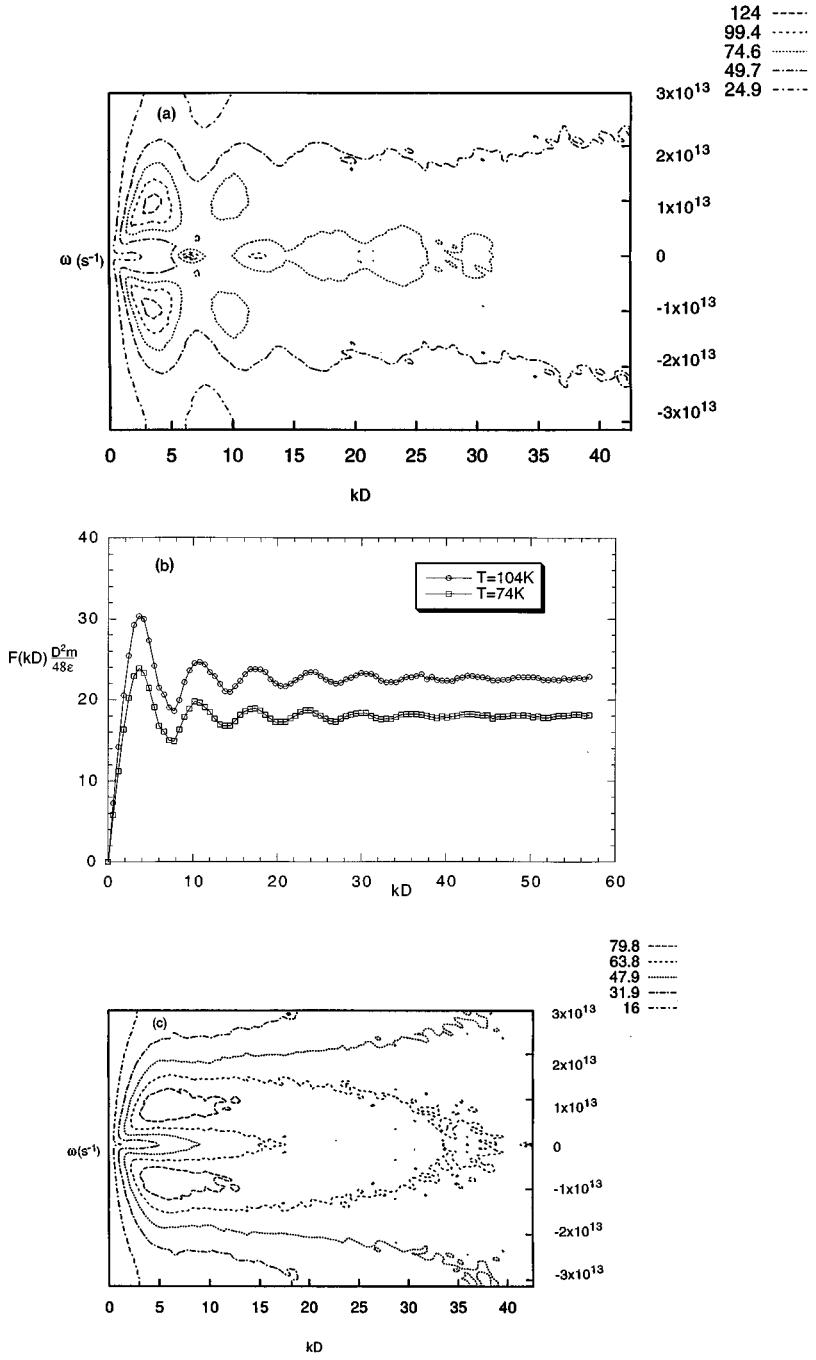

FIG. 2. (a) Isovalues of $|F(k,\omega)|(D^2m/48\varepsilon)$ for $T^*=0.872$, (b) the static Lennard-Jones force spectra $|F(k)|(D^2m/48\varepsilon)$ for $T^*=0.872$ and 0.643, (c) isovalues of $|F_t(k,\omega)|(D^2m/48\varepsilon)$ for $T^*=0.872$.

and valleys along the k axis match the positions of the peaks and valleys for $|N(k,\omega)|$. But, for $|\omega|>0$ only when ω is smaller than a critical value $\omega_c(k)$ the valleys of $|F(k,\omega)|$ are at the blocked wave numbers. Also note that even for $|\omega|>\omega_c(k)$ there is a well-defined structure in $|F(k,\omega)|$, but its form is different. We will discuss the reasons for these changes in the structure of $|F(k,\omega)|$ later in this section.

We next study the spectrum of the area-averaged transverse force $|F_t(k,\omega)|$ shown in Fig. 2(c) for $T=104$ K. From this figure we note that $F_t(k,\omega)$ is maximum at ($kD=5.39$, $\omega=9.6\times10^{12}$ s), but for $\omega=0$ it is relatively small and the structure we have seen in $|N(k,\omega)|$ and $|F(k,\omega)|$ is missing. The qualitative structure of $F_t(k,\omega)$ is therefore different from the structure we have seen in $N(k,\omega)$ and $F(k,\omega)$. The magnitude of the maximum and the values of k and ω at the maximum are, however, comparable to their respective values for $F(k,\omega)$. This implies that the transverse and longitudinal Lennard-Jones force fields act to drive comparable wave numbers at comparable frequencies.

The phase difference between the Lennard-Jones force and number density spectra $P_{FN}(k,\omega)$ is shown in Fig. 3(a)–(b) for two different values of the reduced temperature. From these figures we note that for every wave number $kD>\sim2.0$ there is a unique frequency $\omega_c(k)$ at which the phase difference $P_{FN}(k,\omega)$ changes sign. Specifically, for $\omega<\omega_c(k)$, $P_{FN}(k,\omega)$ is approximately $\pi/2$, and for $\omega>\omega_c(k)$ is approximately $-\pi/2$. This result for the direct numerical simulations agrees with the result obtained earlier from Eqs. (3.5) and (3.6) that the phase difference should be $\pm\pi/2$. Thus the phase constraint required by Eqs. (3.5) and (3.6) is satisfied

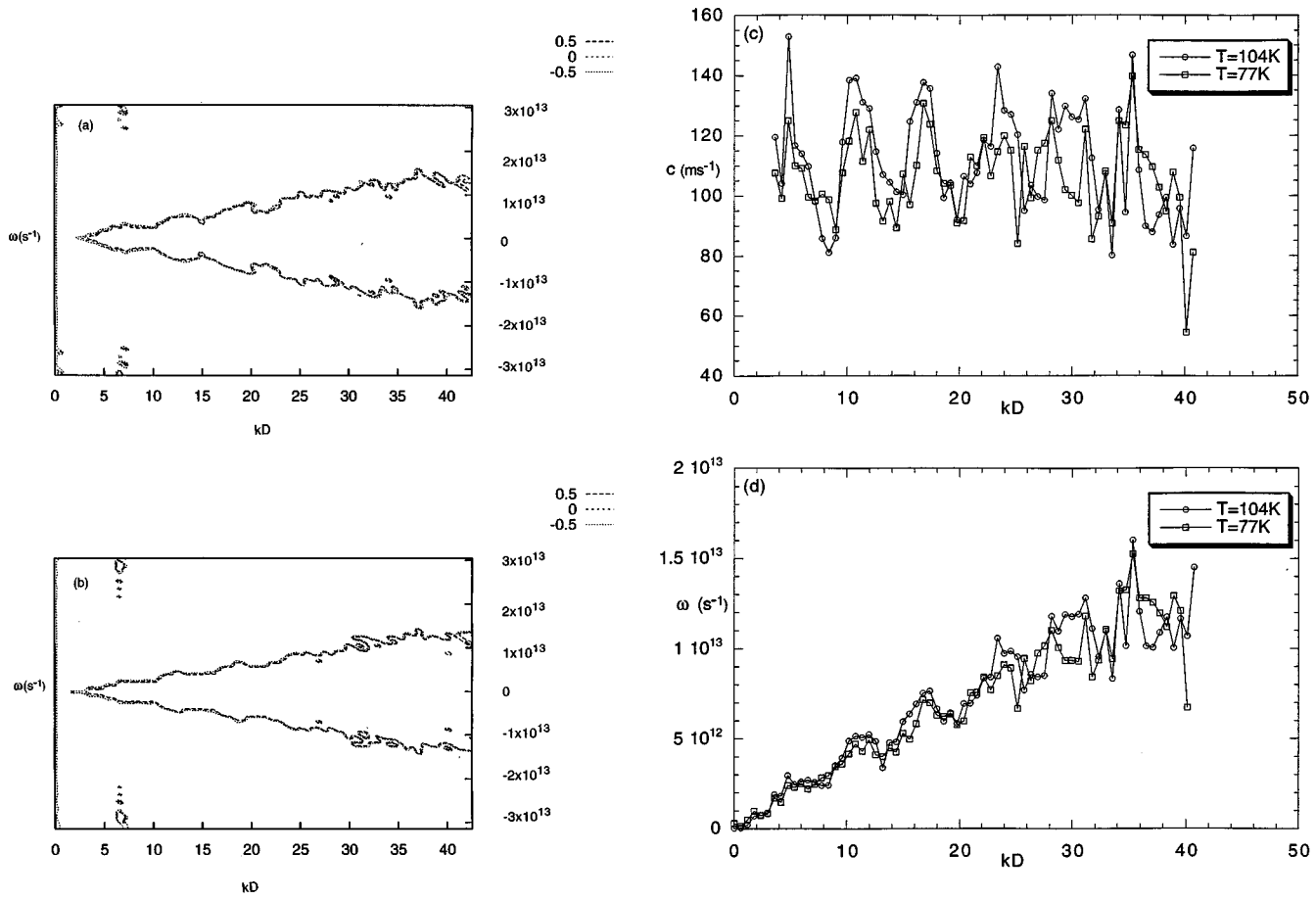

FIG. 3. The phase difference (in radians) between $N(k,\omega)$ and $F(k\omega)$, $P_{FN}(k,\omega)$, is shown. (a) Isovalues for $T^*=0.872$, (b) isovalues for $T^*=0.643$, (c) for the two cases $\omega_c(k)$ is shown as a function of k, (d) for the two cases $c(k)$ is shown as a function of k.

for the numerical simulations. The ratio $c(k)=\omega_c(k)/k$ is defined to be an effective sound speed of the particle system. In Figs. 3(c) and 3(d) we have plotted $\omega_c(k)$ and $c(k)$ as functions k for the two cases shown in Fig. 3(a) and 3(b). From these figures we note that $\omega_c(k)$ increases approximately linearly with k, except close to the blocked wave numbers where it is approximately constant or even decreases with k. The effective sound speed $c(k)$, on the other hand, is approximately constant, except close to the blocked wave numbers where its value is locally minimum. Our numerical results also show that the phases of the number density and the transverse force spectra are *not* correlated. Therefore the transverse force field is not driven by $N(z,t)$.

The above results for the phase difference between the longitudinal force and number density fields suggest that the dynamical nature of the particle-particle interaction changes fundamentally at $\omega=\omega_c(k)$. In particular, as we have noted earlier, the local minima of $|F(k,\omega)|$ for $\omega>\omega_c(k)$ are different from the minima of the static structure factor. Along the boundary $\omega=\omega_c(k)$, the magnitude of $F(k,\omega)$ is locally minimum, and thus the dynamics at these wave numbers is dominated by the convection term in Eq. (3.6). We may therefore conclude that the dynamics of waves with speeds greater than $c(k)$, and waves with speeds smaller than $c(k)$, is fundamentally different.

To sort out the possible reasons for this change in the particle dynamics, we next study the spectrum of the convection term $|C_z(k,\omega)|$ shown in Fig. 4. From this figure we first note that the magnitude of the convection term is comparable to the magnitude of $F(k,\omega)$. However, for $kD<\sim 2$ the convection term is relatively small, and therefore in the long wave (hydrodynamic or continuum) limit the convection effects can be neglected. This result is in agreement with the well-known results for this limit. But, for $kD>2$ the convection effects are significant. Furthermore, for a given k, $|C_Z(k,\omega)|$ is maximum for $\omega\sim\omega_c(k)$, where the phase dif-

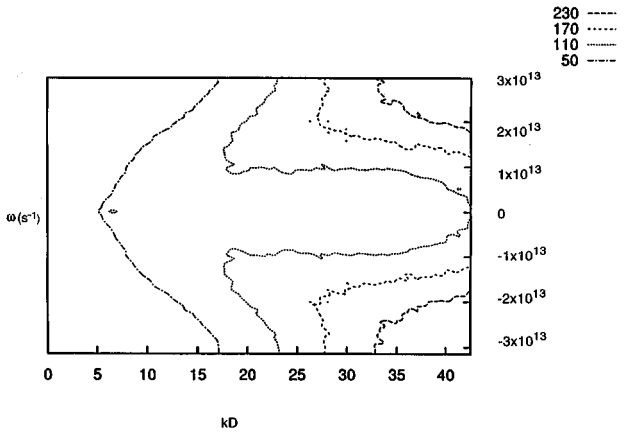

FIG. 4. The magnitude spectrum of $C_Z(k,\omega)(D^2m/48\varepsilon)$ is shown for $T^*=0.872$.

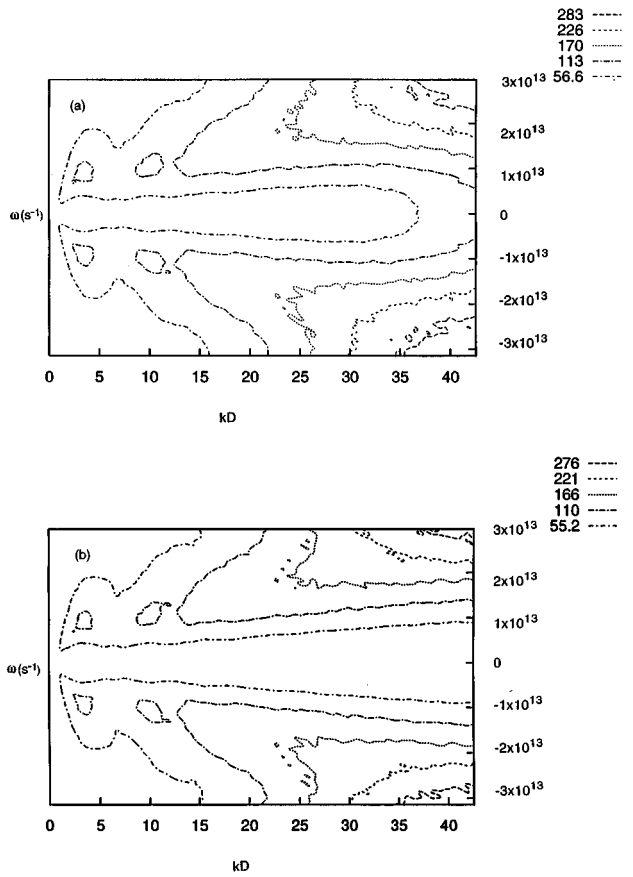

FIG. 5. (a) The magnitude spectrum of the right hand side of (3.6) times $(D^2m/48\varepsilon)$ is shown for $T^*=0.872$, (b) the magnitude spectrum of the left hand side of (3.6) times $(D^2m/48\varepsilon)$ is shown for $T^*=0.872$.

ference between $N(k,\omega)$ and $F(k,\omega)$ changes sign. The convection term, therefore, plays an important role in determining $\omega_c(k)$, and thus cannot be neglected in a theoretical analysis of the particle systems.

Finally, in Fig. 5(a) we study the Fourier spectrum of the sum of the two terms on the right hand side of (3.6). Note in obtaining the sum the phase difference of the two terms is properly taken into account. From this figure we note that the sum is maximum at $\sim$ ($kD=3.39$, $\omega=\pm 1.05\times 10^{13}$ s), and its secondary maximum is at ($kD=10.21$, $\omega=\pm 1.08\times 10^{13}$ s). For $\omega<\omega_c(k)$, however, the sum is relatively small. Therefore, the time derivative of $J(k,\omega)$ is dominated by waves traveling with speeds greater than the effective sound speed. The spectrum of the left hand side of Eq. (3.6) was also obtained *independently*, and is shown in Fig. 5(b). A comparison of Figs. 5(a) and 5(b) shows that the spectra of the left and right hand sides of (3.6) for the direct numerical simulations are approximately identical, including the positions of the primary and secondary maxima, and their values. Finally, we note that the qualitative form of Fig. 5(a) is significantly different from those of the Lennard-Jones force and convection spectra shown in Figs. 2(a) and 4, respectively. This change in the qualitative form is a consequence of the fact that these two terms are of the same approximate magnitude, but the phase difference between them for $\omega<\omega_c(k)$ is π and for $\omega>\omega_c(k)$ is zero. Therefore for $\omega<\omega_c(k)$ the right hand side of (3.6) is relatively small because the convection and Lennard-Jones terms cancel each other. The fact that the sum of these two distributions is the same as the velocity current distribution also demonstrates that the distributions are correct.

V. CHANGE OF TYPE

We have noted in Sec. III that for a Lennard-Jones particle system $F(z,t)$ depends *only* on the instantaneous distribution of $N(z,t)$. The functional dependence of $F(z,t)$ on $N(z,t)$ however, is not known. For our numerical simulations the averaged magnitude spectra of these distributions were presented in the previous section, but the functional relationship between the two is difficult to obtain from the numerical spectra. In the previous section we also noted that the phase difference $P_{FN}(k,\omega)$ between $F(k,\omega)$ and $N(k,\omega)$ depends on k and ω: it is $+\pi/2$ for $\omega<\omega_c(k)$ and $-\pi/2$ for $\omega>\omega_c(k)$. The physical and mathematical significance of this change in the phase difference is difficult to understand because the governing equations are highly nonlinear. In this section we show that this change in the sign of $P_{FN}(k,\omega)$ is a consequence of the change of type of the governing equations, and then discuss the physical significance of this result.

In order to understand the mathematical significance of the change in the sign of $P_{FN}(k,\omega)$, we next do a simple analysis of the governing Eqs. (3.5) and (3.6). We take two approaches: in one we drop the nonlinear convection term but carry the full form of the force term, and in the other we keep the convection term, but linearize the force term. In both cases the result obtained is the same. In the first approach we use the fact that the phase difference between $F(k,\omega)$ and $N(k,\omega)$ is known to write $F(k,\omega)$ as

$$F(k,\omega)=\exp\left\langle \pm i\,\frac{\pi}{2}+i\ \arg[N(k,\omega)]\right\rangle |F(k,\omega)|,$$

where the plus sign applies when $\omega<\omega_c$, and the minus sign applies when $\omega>\omega_c$. We next substitute this form for $F(k,\omega)$ in the Fourier transform of the linearized (3.6). The resulting equation can be written as

$$i\omega J(k,\omega)=\exp\left\langle \pm i\,\frac{\pi}{2}+i\ \arg[N(k,\omega)]\right\rangle |F(k,\omega)|.$$

From the above equations, $J(k,\omega)$ can be eliminated by using the Fourier transform of Eq. (3.5): $ik\ J(k,\omega)=i\omega N(k,\omega)$. The resulting equation, after some manipulations can be written as

$$i\,\frac{\omega^2}{k}\,N(k,\omega)=\exp\left\langle \pm i\,\frac{\pi}{2}+i\ \arg[N(k,\omega)]\right\rangle |F(k,\omega)|.$$

This equation can be simplified further if we note

$$N(k,\omega)=\exp(i\ \arg[N(k,\omega)])|N(k,\omega)|,$$

and cancel $\exp(i\ \mathrm{arc}[N(k,\omega)])$ from the two sides. After this cancellation, we get

$$\frac{\omega^2}{\alpha}=\exp\left(\pm i\,\frac{\pi}{2}-i\,\frac{\pi}{2}\right)\frac{|F(k,\omega)|}{|N(k,\omega)|}.$$

The above equation can now be solved for ω,

$$\omega = \sqrt{k}\left[\frac{|F(k,\omega)|}{|N(k,\omega)|}\right]^{1/2} \quad \text{for } \omega > \omega_c$$

$$= i\sqrt{k}\left[\frac{|F(k,\omega)|}{|N(k,\omega)|}\right]^{1/2} \quad \text{for } \omega < \omega_c .$$

Therefore the characteristics are imaginary for $\omega<\omega_c$, and real for $\omega>\omega_c$. This implies that the governing equations are elliptic for $\omega<\omega_c$, and hyperbolic for $\omega>\omega_c$ (see Courant and Hilbert [16]).

In the second approach, we assume the following form for $F(z,t)$:

$$F(z,t) = \pm K \frac{\partial}{\partial z} N(z,t), \tag{5.1}$$

where $K>0$ is the coefficient of linearization, and the minus sign applies when $\omega>\omega_c$ and the plus sign applies when $\omega<\omega_c$. Clearly, the above relationship between $F(z,t)$ and $N(z,t)$ satisfies the two requirements we have stated earlier, i.e., $F(z,t)$ depends on $N(z,t)$, and the phase difference between $F(z,t)$ and $N(z,t)$ is $\pm\pi/2$. Note in the long wave limit Eqs. (3.5), (3.6), and (5.1) with the minus sign are mathematically identical to the equations in gas dynamics: $(\partial\rho/\partial t)+(\partial u\rho/\partial z)=0$; and $(\partial u\rho/\partial t)+(\partial uu\rho/\partial z = -c^2(\partial\rho/\partial z)$, where ρ is the density and c is the speed of sound. The next step is to substitute the above form for $F(z,t)$ in (3.6), and find the characteristic directions of (3.5) and (3.6) (see Courant and Hilbert [16], and Whitham [17]). It is easy to show that the characteristic directions are given by

$$\frac{dz}{dt} = u \pm \sqrt{\pm(-K)}.$$

Therefore, the characteristics are real, and the system is hyperbolic, when the minus sign is used in (5.1). Since our numerical results show that for $kD<\sim 2$, the minus sign holds for all ω's, in the long wave limit Eqs. (3.5) and (3.6) are hyperbolic. The equations in gas dynamics are also hyperbolic. A direct comparison of (3.5) and (3.6) with equations in gas dynamics shows that the change of sign in (5.1) is equivalent to assuming that the functional dependence of the pressure field on the gradient of the density field changes sign.

The mathematical properties of the elliptic and hyperbolic system of equations are well known, and are given in any elementary book on the partial differential equations (see Courant and Hilbert [16] and Weinberger [18]). We briefly note that for an elliptic system the local solution depends on the overall distribution in the domain and the problem is well posed only if it is posed as a boundary value problem. On the other hand, for a hyperbolic system the local solution depends only on the distribution along the upstream portion of the characteristic passing through the point under consideration. We remind the reader that the exact dynamics of the system of particles is governed by Eq. (3.1), and $P_{FN}(k,\omega)$ is obtained by solving these equations. Therefore, there is a fundamental change in the particle dynamics at $\omega=\omega_c(k)$ which, in principle, can be observed in an experiment designed to study the phase differences. These experimental results for the phase differences can also be used to check the validity of the Lennard-Jones model for the real fluids.

In conclusion, the above discussion suggests that the change in the sign of $P_{FN}(k,\omega)$ at $\omega=\omega_c(k)$ is a result of the change in type of the governing Eqs. (3.5) and 3.6). Furthermore, for $kD>\sim 2$ (or wavelength $\lambda<\sim 3D$) the area-averaged distributions for slowly moving waves are governed by an elliptic system of equations. This suggests that the change of type is a *finite* size effect because it exists only for wavelengths comparable or smaller than D. It is, however, difficult to give a *precise* reason from a physical point of view for this fundamental change in the particle dynamics. One possible explanation for this change is that as a particle of diameter D moves, its motion is instantaneously felt within the volume occupied by the sphere. In a theory based on the particle centers this instantaneous transmission of the change in the position and velocity of the particle center, up to a distance $D/2$ from the center, gives rise to the elliptic behavior observed for λ's comparable or smaller than D. For long waves ($kD<\sim 2$) this effect does not exist for any frequency, and thus the response of the particle system in this limit is consistent with that of a compressible fluid.

VI. CONCLUSIONS

We have studied the time-averaged Fourier spectra of the number density, velocity, convection, and force fields for an assembly of spherical particles interacting via the Lennard-Jones potential. The results were obtained numerically by solving the equations for the particles in a periodic domain. A detailed study of the phase difference between the Lennard-Jones force and number density spectra shows that for every wave number there is a unique frequency at which the phase difference changes from $\pi/2$ to $-\pi/2$. A simple analysis shows that the change in the sign of the phase difference implies a change of type of the governing partial differential equations from hyperbolic to elliptic. This fundamental change in the particle dynamics is also reflected in the qualitative forms of the spectra. In particular, the maxima and minima of the Lennard-Jones force field are the same as for the static structure factor only for waves with speeds less than the effective sound speed. Finally, we note that the convection effects are of the same order of magnitude as the Lennard-Jones forces, and therefore must be included in a mathematical model of the particle systems. The numerical results for the phase difference and convection spectrum are interesting, and should be compared with the analytical results where the nonlinear convection term is retained as well as with the experimental data for the real liquids. At present, however, this comparison is not possible because these analytical and experimental results are not available.

APPENDIX

In this appendix we briefly discuss the results obtained by Singh [12], and Singh and Joseph [13–15] for the area fraction, and their importance in the interpretation of the diffraction data. They have obtained the following expression for the area fraction ϕ_a in terms of $N(z,t)$ (see the derivation

given in these references for a better physical understanding of this equation)

$$\phi_a(z,t)=\int_{-R}^{R} N(x+z,t)\,\pi(R^2-x^2)\,dx, \tag{A1}$$

where R is the radius of the particles. Using this expression they have shown that when N is the Fourier transform class, then

$$\phi_a(k,t)=\frac{4\pi R^3}{3}\,\Theta(kR)N(k,t), \tag{A2}$$

where $\Theta(kR)=3[\sin kR/(kR)^3-\cos kR/(kR)^2]$ is the blockage function and $\phi_a(k,t)$ is the Fourier transform of $\phi_a(z,t)$. Note that $\Theta(kR)=J_{1/2}(kR)/kR$, where $J_{1/2}$ is the spherical Bessel function of order 1/2. The set of zeros of $\Theta(kR)$ is: $2kR=8.98,\ 15.45,\ 21.81,\ldots$. From (A2) Singh and Joseph have concluded that when the number density is in the Fourier transform class, then the dimensionless wave numbers, kR, for which $\Theta(kR)$ is zero, are *blocked* (i.e., are missing) in the spectrum of the area fraction. We would refer to these wave numbers as ''blocked wave numbers.''

The above result for the area fraction is also useful in the interpretation of diffraction data. Specifically, the angular distribution of the scattered intensity $I(\theta,t)$ can be related to the area-averaged one-dimensional spatial distribution of the area fraction, where θ is the angle at which the intensity is measured. In order to show this, we start with the following well-known expression that relates the spatial distribution of the scattering density $s(\mathbf{r},t)$ to the scattered (elastic) intensity (see Cowley [19])

$$I(\theta,t)\sim\left|\int_V s(\mathbf{r},t)\exp(i\mathbf{k}\cdot\mathbf{r})\,d\mathbf{r}\right|^2.$$

Here the integral is over the scattering volume V and $s(\mathbf{r},t)$ is zero outside of the particle, and the angle $\theta=\sin^{-1}(k\lambda/4\pi)$ where λ is the wave length of the radiation used and $\mathbf{k}$ is the wave number being explored. Let us assume that our coordinate system is such that $\mathbf{k}\cdot\mathbf{r}=kz$, i.e., the z axis of the coordinate system is parallel to the scattering vector $\mathbf{k}$. Then, the above expression reduces to

$$\begin{aligned} I(\theta,t)&\sim\left|\int_z\left[\int_x\int_y s(\mathbf{r},t)\,dx\,dy\right]\exp(ikz)\,dz\right|^2\\ &=\left|\int_z s_a(z,t)\exp(ikz)\,dz\right|^2, \end{aligned} \tag{A3}$$

where $s_a(z,t)=\int_x\int_y s(\mathbf{r},t)\,dx\,dy$ is the area average of the scattering density. If we assume that the scattering density $s(\mathbf{r},t)=s_0$ is uniform within the particles, then $s_a(z,t)=ps_0\phi_a(z,t)$, where p is the area over which the averaging is performed. In this case, after using (A2) we get

$$I(\theta,t)\sim p^2s_0^2|\phi_a(k,t)|^2=p^2s_0^2\left[\frac{4\pi R^3}{3}\right]^2\Theta^2(kR)|N(k,t)|^2, \tag{A4}$$

where $\Theta(kR)$ is the form factor for a single particle. The form factor is the *same* as the blockage function because the scattering density is uniformly distributed within the particles. Furthermore, from (2.8) we already know that when $\langle\rho(\mathbf{r})\rangle$ is radially symmetric, then $\langle|\rho(\mathbf{k})|^2\rangle$ is proportional to $\langle|N(k)|^2\rangle$. Therefore an estimate of $\langle|\rho(\mathbf{k})|^2\rangle$ can be obtained from the angular distribution of the time-averaged scattered intensity $\langle I(\theta)\rangle$. Also note that even when $\langle\rho(\mathbf{r})\rangle$ is anisotropic $\langle I(\theta)\rangle$ is related to the area-averaged distribution along the scattering vector [see (A3)]. A complete picture of the anisotropic distribution, however, is much more difficult to obtain. But, in principle, its approximate form can be obtained by using a deconvolution algorithm on a set of data obtained for different orientations of the scattering vector.

The physical significance of $\langle I(\theta)\rangle$ in (A3) and (A4) is usually given in terms of the radially symmetric distributions. In particular, the time average of the angular distribution $\langle I(\theta)\rangle$ is described to be the product of the form factor and the radially symmetric structure factor. The form factor of a single particle is then filtered out of $\langle I(\theta)\rangle$, because it does not have any dynamical significance, to give the structure factor. This explanation, however, fails to stress the fact that $\langle I(\theta)\rangle$ is related to the time average of the Fourier transform of the area-averaged scattering density. Even more importantly, it fails to emphasize that when $s(\mathbf{r},t)=s_0$ within the particles, the zeros of $\langle I(\theta)\rangle$ are indicative of the fundamental property that the spatial Fourier transform of the area covered by the particles *cannot* contain the blocked wave numbers [see Eq. (A4)]. Finally, we note that if in the scattering experiments we *only* have access to the intensities, i.e., the magnitude squared of the Fourier transform of the distribution functions, the phase of the distributions *cannot* be studied experimentally which, as we shown in this paper, contains important information about the dynamics of the particle systems.

I wish to thank Dr. Todd Hesla for his constructive criticism of the paper.

[1] L. Verlet, Phys. Rev. **165**, 201 (1968).
[2] D. Chandler, *Introduction to Modern Statistical Mechanics* (Oxford University Press, New York, 1987).
[3] J. P. Hansen and I. R. McDonald *Theory of Simple Liquids* (Academic, New York, 1990).
[4] J. P. Boon and S. Yip, *Molecular Hydrodynamics* (Dover, New York, 1991).
[5] P. N. Pusey, J. Phys. A Math. Nucl. Gen. **11**, 119 (1978).
[6] M. P. Wai, R. A. Gelman, M. G. Fatica, R. H. Hoerl, and G. D. Wignall, Polymer **28**, 918 (1987).

[7] G. D. Wignall, V. R. Ramakrishanan, M. A. Linne, A. Klein, L. H. Sperling, M. P. Wai, R. A. Gelman, M. G. Fatica, R. H. Hoerl, L. W. Fisher, S. M. Melpolder, and J. M. O'Beilly, Mol. Cryst. Liq. Cryst. A **180**, 25 (1990).
[8] N. S. Gingrich, Rev. Mod. Phys. **15**, 90 (1993).
[9] R. F. Kruh, Chem. Rev. **62**, 319 (1962).
[10] J. L. Yarnell, M. J. Katz, R. G. Wenzel, and S. H. Koeing, **7**, 2130 (1973).
[11] R. H. Ottewill, J. Appl. Cryst. **24**, 436 (1991).
[12] P. Singh, Ph.D. thesis, University of Minnesota, 1991.
[13] P. Singh and D. D. Joseph, *Two Phase Flows in Fluidized Beds, Sedimentation and Granular Flows*, IMA Volumes in Mathematics and its Applications Vol. 26 (Springer-Verlag, Berlin, 1990), pp. 130, 149.
[14] P. Singh and D. D. Joseph, Am. Soc. Mech. Eng. 77 (1991).
[15] P. Singh and D. D. Joseph, Int. J. Multiphase Flows **21**, 1(1995).
[16] Courant and Hilbert, *Methods of Mathematical Physics* (Wiley, New York, 1989), Vol. II.
[17] G. B. Whitman, *Linear and Nonlinear Waves* (Wiley, New York, 1974).
[18] H. F. Weinberger, *A First Course in Partial Differential Equations* (Wiley, New York, 1965).
[19] J. M. Cowley, *Diffraction Physics* (North-Holland, Amsterdam, 1990).